JOURNAL OF COMPUTATIONAL PHYSICS 118, 109–119 (1995)

A Fractional-Step Method for Solving 3D, Time-Domain Maxwell Equations

J. S. SHANG*

Flight Dynamics Directorate, Wright Laboratory, Wright-Patterson Air Force Base, Ohio

Received February 1, 1993; revised August 10, 1994

Stable and efficient implicit and explicit fractional-step methods for solving three-dimensional, time-dependent Maxwell equations have been successfully developed. These numerical procedures are characteristic-based schemes with the intrinsically accurate no-reflection wave condition on the boundaries of truncated computational domain. Excellent simulations for electromagnetic phenomena have been achieved for a three-dimensional wave guide and an oscillating electric dipole.

I. INTRODUCTION

Recent progress in computational electromagnetics has created a new frontier for research in plasmadynamics, optical pulses, and electromagnetic wave propagation, as well as the interface between classical electrodynamics and quantum mechanics [1, 2]. In this scientific endeavor, efforts are required to numerically solve the time dependent Maxwell equations for propagating and scattering electromagnetic waves [2–5]. The system of partial differential equations to be solved is hyperbolic and constitutes an initial-value problem [6]. For all finite-difference or finite-volume approximations of the Maxwell equations, a fundamental difficulty arises from the necessity of imposing boundary values on a truncated computational domain to an initial-value system. These artificial boundaries will induce wave reflections. In addition to degrading the accuracy of interacting wave patterns, the reflecting waves from the artificial boundaries also contribute to erroneous accumulations of radiating energy. The distortion of energy content leads to unrealistic modulations of the amplitude of wave motion [5]. Despite numerous attempts to alleviate this difficulty, approximated boundary conditions are still inherently limited as applied to the total field. Only the compatibility conditions which are derived from the characteristics can completely eliminate the spurious wave reflection at the truncated spatial domain [3, 4, 6–8].

Another urgent need in computational electromagnetics is the improvement of numerical efficiency. For wave propagation phenomena, the numerical resolution of wave motions is dictated by the minimum wave number within the frequency spectrum. In order to provide adequate numerical resolution for frequency ranges beyond the Rayleigh into the resonance and optical regimes, the required number of discretized data nodes is enormous [1, 2, 5]. In radar cross section computation of aerospace vehicles, a desirable predictive dynamic range can be as high as 60 dB over broad angular ranges [1]. The stringent requirement of computational electromagnetics can be met only by low reflection coefficient radiation boundary conditions and a very efficient numerical algorithm. The aggregated consequence is that large amounts of data usually must be processed by a conditionally stable numerical algorithm which limits our capability in this area of scientific endeavor. A possible alternative may be derived from the characteristic-based numerical schemes developed to solve the Euler equations in computational fluid dynamics [9, 10]. In a previous effort, three characteristic-based algorithms were devised for solving the time-domain Maxwell equations [3, 4]. Not only is the numerical stability constraint removed from the solving scheme, the perfect shift condition [11] is also achieved in one-dimensional space by both explicit and implicit methods. At the Courant numbers of one and two, solutions of a simple wave generated by the numerical method are devoid of any aliasing numerical errors on a uniformly spaced mesh system.

The fundamental idea of the characteristic-based methods, either the flux vector splitting or flux difference splitting [9, 10], for solving hyperbolic equation systems is derived from eigenvalue analysis. In numerical analysis, the well-posedness requirement and the stability of a discretized system are ultimately linked to eigenvalues of governing equations. Therefore, characteristic-based schemes have shown a drastic improvement to numerical stability and accuracy by using a windward difference formulation to solve the initial value problems [9, 10]. In short, the solving procedure is developed to mimic the wave mechanism of information propagation [10]. However, the characteristic-based algorithm also has an inherent limitation in that the coefficient matrices of the governing equations, when written in flux vector form, can be diagonalized in only

* The U.S. Government's right to retain a nonexclusive royalty-free license in and to the copyright covering this paper, for governmental purposes, is acknowledged.

0021-9991/95 $6.00

one dimension at a time. In previous efforts [3, 4], all multidimensional equations are split into multiple one-dimensional formulations and solved by alternating direction implicit (ADI) schemes [12–14]. This general approach has been successfully applied to solve two-dimensional time-domain Maxwell equations [4]. However, its extension to three-dimensional applications has been proven to be inefficient due to the rather restrictive numerical stability property of the ADI algorithm for solving the three-dimensional, time-dependent Maxwell equations [3].

The present effort sustains the pursuit in developing an efficient characteristic-based algorithm for solving three-dimensional Maxwell equations in time domain. A major point of departure from the earlier efforts is focused on the manner in which the multidimensional calculations were carried out. In essence, the ADI scheme [3, 4, 15] is replaced by the fractional-step or the splitting approximation [16, 17]. The splitting scheme has provided a superior stability property than that of ADI to the hyperbolic system. It is known that the spatially central ADI formulation of hyperbolic systems is unconditionally unstable [18, 19]. The numerical stability can be improved by using a windward difference, but the stability constraint is still too limited for efficient applications [4]. The splitting scheme is closely related to, in some cases identical with, the ADI methods [11, 14]. The main difference lies in the treatment of the off-diagonal difference operators. The fractional-step method retains only the diagonal difference operator in the numerical sweep directions. Consequently, for any scalar equation, the amplification factor is simply the product of the amplification factors of the one-dimensional equations [14, 16, 17]. Once the stability restriction is removed, the present investigation will be focused on the issues of numerical accuracy and no-reflection numerical boundary conditions.

II. ANALYSIS

II.1. *Basic Formulation*

The relevant time-dependent Maxwell equations for electromagnetic field in free space [20] can be written in the form:

$$\frac{\partial(\mu H)}{\partial t} + \nabla \times E = 0 \tag{1}$$

$$\frac{\partial(\varepsilon E)}{\partial t} - \nabla \times H = -J. \tag{2}$$

The system of equations expressed in vector form on a Cartesian frame are

$$\frac{\partial U}{\partial t} + A\frac{\partial U}{\partial x} + B\frac{\partial U}{\partial y} + C\frac{\partial U}{\partial z} = -J, \tag{3}$$

where the coefficient matrices (Jacobian of flux vector) A, B, and C are

$$A = \begin{bmatrix} 0 & 0 & 0 & 0 & 0 & 0 \\ 0 & 0 & 0 & 0 & 0 & 1/\varepsilon \\ 0 & 0 & 0 & 0 & -1/\varepsilon & 0 \\ 0 & 0 & 0 & 0 & 0 & 0 \\ 0 & 0 & -1/\mu & 0 & 0 & 0 \\ 0 & 1/\mu & 0 & 0 & 0 & 0 \end{bmatrix} \tag{4}$$

$$B = \begin{bmatrix} 0 & 0 & 0 & 0 & 0 & -1/\varepsilon \\ 0 & 0 & 0 & 0 & 0 & 0 \\ 0 & 0 & 0 & 1/\varepsilon & 0 & 0 \\ 0 & 0 & 1/\mu & 0 & 0 & 0 \\ 0 & 0 & 0 & 0 & 0 & 0 \\ -1/\mu & 0 & 0 & 0 & 0 & 0 \end{bmatrix} \tag{5}$$

$$C = \begin{bmatrix} 0 & 0 & 0 & 0 & 1/\varepsilon & 0 \\ 0 & 0 & 0 & -1/\varepsilon & 0 & 0 \\ 0 & 0 & 0 & 0 & 0 & 0 \\ 0 & -1/\mu & 0 & 0 & 0 & 0 \\ 1/\mu & 0 & 0 & 0 & 0 & 0 \\ 0 & 0 & 0 & 0 & 0 & 0 \end{bmatrix} \tag{6}$$

$$U = [E_x, E_y, E_z, H_x, H_y, H_z] \tag{7}$$

$$J = [J_x, J_y, J_z, 0, 0, 0]^T, \tag{8}$$

where ε and μ are the electric permittivity and magnetic permeability which relate the electric flux density to the electric field intensity and the magnetic flux density to the magnetic field intensity, respectively.

The eigenvalues of the coefficient matrices A, B, and C are identical, but they contain multiplicities. Despite that, linearly independent eigenvectors can still be found [3, 4]. The matrix A (or B or C) may be independently diagonalized by a straightforward matrix multiplication,

$$\text{Diag}(\lambda) = \left\{\frac{1}{\sqrt{\mu\varepsilon}}, \frac{1}{\sqrt{\mu\varepsilon}}, -\frac{1}{\sqrt{\mu\varepsilon}}, -\frac{1}{\sqrt{\mu\varepsilon}}, 0, 0\right\} \tag{9}$$

$$D_x = S_x^{-1} A S_x \tag{10}$$

$$D_y = S_y^{-1} B S_y \tag{11}$$

$$D_z = S_z^{-1} C S_z, \tag{12}$$

where S is a nonsingular similar matrix constructed by the eigenvectors as the column vector and S^{-1} is its left-hand inverse. Identical procedures are also performed to the coefficient matrix of other coordinates of the Cartesian frame. Similar

matrices associated with each of the coefficient matrices A, B, and C are given by

$$S_x = \begin{bmatrix} 0 & 0 & 0 & 0 & 0 & 1 \\ \sqrt{\mu/\varepsilon} & 0 & -\sqrt{\mu/\varepsilon} & 0 & 0 & 0 \\ 0 & -\sqrt{\mu/\varepsilon} & 0 & \sqrt{\mu/\varepsilon} & 0 & 0 \\ 0 & 0 & 0 & 0 & 1 & 0 \\ 0 & 1 & 0 & 1 & 0 & 0 \\ 1 & 0 & 1 & 0 & 0 & 0 \end{bmatrix} \tag{13}$$

$$S_y = \begin{bmatrix} -\sqrt{\mu/\varepsilon} & 0 & \sqrt{\mu/\varepsilon} & 0 & 0 & 0 \\ 0 & 0 & 0 & 0 & 1 & 0 \\ 0 & \sqrt{\mu/\varepsilon} & 0 & -\sqrt{\mu/\varepsilon} & 0 & 0 \\ 0 & 1 & 0 & 1 & 0 & 0 \\ 0 & 0 & 0 & 0 & 0 & 1 \\ 1 & 0 & 1 & 0 & 0 & 0 \end{bmatrix} \tag{14}$$

$$S_z = \begin{bmatrix} \sqrt{\mu/\varepsilon} & 0 & -\sqrt{\mu/\varepsilon} & 0 & 0 & 0 \\ 0 & -\sqrt{\mu/\varepsilon} & 0 & \sqrt{\mu/\varepsilon} & 0 & 0 \\ 0 & 0 & 0 & 0 & 1 & 0 \\ 0 & 1 & 0 & 1 & 0 & 0 \\ 1 & 0 & 1 & 0 & 0 & 0 \\ 0 & 0 & 0 & 0 & 0 & 1 \end{bmatrix} \tag{15}$$

where the ratio $\sqrt{\mu/\varepsilon}$ is referred to as the intrinsic impedence of the medium [20].

For the present investigation and without loss of generality, the propagating waves are confined in isotropic media separated by a physical interface. Under these conditions, the permittivity and permeability are assigned constant values [3, 4, 20]. Thus, the left-hand inverse of the similarity transformation matrix S^{-1} can be brought into the differentiation with respect to both time and space. The resulting equations are completely uncoupled from each other [3, 4]. These independent and scalar equations describe the invariant characteristic variables along trajectories with slopes defined by their associated eigenvalues. Since one-dimensional characteristic equations are completely uncoupled, the system of equations can be solved individually. The windward differencing approximation decomposes the matrix system into upper and lower tridiagonal structures, according to the sign of the eigenvalue. Only a single numerical sweep is required to solve the complete discretized equations system. For an implicit solving scheme, the costly pentadiagonal inversion procedure becomes unnecessary and leads to a very efficient numerical procedure.

All one-dimensional characteristic variables in each coordinate can be given as

$$W_x = S_x^{-1} U$$

$$S_x^{-1} = \begin{bmatrix} 0 & \sqrt{\varepsilon/\mu}/2 & 0 & 0 & 0 & 1/2 \\ 0 & 0 & -\sqrt{\varepsilon/\mu}/2 & 0 & 1/2 & 0 \\ 0 & -\sqrt{\varepsilon/\mu}/2 & 0 & 0 & 0 & 1/2 \\ 0 & 0 & \sqrt{\varepsilon/\mu}/2 & 0 & 1/2 & 0 \\ 0 & 0 & 0 & 1 & 0 & 0 \\ 1 & 0 & 0 & 0 & 0 & 0 \end{bmatrix} \tag{16}$$

$$W_y = S_y^{-1} U$$

$$S_y^{-1} = \begin{bmatrix} -\sqrt{\varepsilon/\mu}/2 & 0 & 0 & 0 & 0 & 1/2 \\ 0 & 0 & \sqrt{\varepsilon/\mu}/2 & 1/2 & 0 & 0 \\ \sqrt{\varepsilon/\mu}/2 & 0 & 0 & 0 & 0 & 1/2 \\ 0 & 0 & -\sqrt{\varepsilon/\mu}/2 & 1/2 & 0 & 0 \\ 0 & 1 & 0 & 0 & 0 & 0 \\ 0 & 0 & 0 & 0 & 1 & 0 \end{bmatrix} \tag{17}$$

$$W_z = S_z^{-1} U$$

$$S_z^{-1} = \begin{bmatrix} \sqrt{\varepsilon/\mu}/2 & 0 & 0 & 0 & 1/2 & 0 \\ 0 & -\sqrt{\varepsilon/\mu}/2 & 0 & 1/2 & 0 & 0 \\ -\sqrt{\varepsilon/\mu}/2 & 0 & 0 & 0 & 1/2 & 0 \\ 0 & \sqrt{\varepsilon/\mu}/2 & 0 & 1/2 & 0 & 0 \\ 0 & 0 & 1 & 0 & 0 & 0 \\ 0 & 0 & 0 & 0 & 0 & 1 \end{bmatrix}. \tag{18}$$

Therefore in each coordinate direction, the time-dependent, three-dimensional Maxwell equations are uncoupled into six independent scalar equations according to their associated eigenvalues. For $n = 1, 2, \ldots, 6$,

$$L_x: \frac{\partial W_{x,n}}{\partial t} + \lambda_n \frac{\partial W_{x,n}}{\partial x} = 0 \tag{19}$$

$$L_y: \frac{\partial W_{y,n}}{\partial t} + \lambda_n \frac{\partial W_{y,n}}{\partial y} = 0 \tag{20}$$

$$L_z: \frac{\partial W_{z,n}}{\partial t} + \lambda_n \frac{\partial W_{z,n}}{\partial z} = 0. \tag{21}$$

From the sign of the eigenvalue, the stencil of second-order accurate windward difference approximation can be easily con-

structed to form the one-dimensional difference operators, if $\lambda < 0$,

$$\frac{\partial W}{\partial x} = \frac{-3W_{i,j,k} + 4W_{i+1,j,k} - W_{i+2,j,k}}{2\Delta x}; \tag{22}$$

if $\lambda > 0$,

$$\frac{\partial W}{\partial x} = \frac{3W_{i,j,k} - 4W_{i-1,j,k} + W_{i-2,j,k}}{2\Delta x}. \tag{23}$$

II.2. *Accuracy of Time Integration*

The three-dimensional system is solved by the fractional-step or time splitting scheme as previously mentioned [14, 16, 17]. In its most elementary form, the fractional-step method is given as

$$W^{n+2} = L_x L_y L_z L_z L_y L_x W^n. \tag{24}$$

The symmetric and cyclic sequence of one-dimensional operators is designed to retain the second-order accuracy in space and time [14, 16, 17]. The one-dimensional characteristics W_x, W_y, and W_z are distinct in different coordinates. Therefore, during the cyclic computing sequence, a dependent variable transformation was performed to convert the characteristics from one temporal-spatial plane to the other. The relationship between the three sets of characteristics is explicit and can be given as

$$W_x = S_x^{-1} S_y W_y = S_x^{-1} S_z W_z \tag{25}$$

$$W_y = S_y^{-1} S_x W_x = S_y^{-1} S_z W_z \tag{26}$$

$$W_z = S_z^{-1} S_x W_x = S_z^{-1} S_y W_y. \tag{27}$$

Nevertheless the system of one-dimensional characteristic equations (19), (20), and (21) is identical to

$$L_x; \frac{\partial U}{\partial t} + A\frac{\partial U}{\partial x} = 0 \tag{28}$$

$$L_y; \frac{\partial U}{\partial t} + B\frac{\partial U}{\partial y} = 0 \tag{29}$$

$$L_z; \frac{\partial U}{\partial t} + C\frac{\partial U}{\partial z} = 0. \tag{30}$$

The temporal second-order accurate approximations of these one-dimensional difference operators are derived from the Taylor series expansion in time,

$$L_x; U^{n+1} = U^n + \left(\frac{\partial U}{\partial t}\right)\Delta t + \frac{1}{2}\left(\frac{\partial^2 u}{\partial t^2}\right)\Delta t^2 + O(\Delta t^3)$$

$$\frac{\partial U}{\partial t} = -\frac{\partial F}{\partial x} = -A\frac{\partial U}{\partial x}$$

$$\frac{\partial^2 U}{\partial t^2} = \frac{\partial}{\partial t}\left(-\frac{\partial F}{\partial x}\right) = -\frac{\partial}{\partial x}\left(\frac{\partial F}{\partial t}\right) = -\frac{\partial}{\partial x}\left(\frac{\partial F}{\partial U}\frac{\partial U}{\partial t}\right) \tag{31}$$

$$= \frac{\partial}{\partial x}\left(AA\frac{\partial U}{\partial x}\right)$$

$$U^{n+1} = U^n - A\left(\frac{\partial U}{\partial x}\right)\Delta t + \frac{1}{2}\frac{\partial}{\partial x}\left(AA\frac{\partial U}{\partial x}\right)\Delta t^2 + O(\Delta t^3)$$

Similarly,

$$L_y; U^{n+1} = U^n - B\left(\frac{\partial U}{\partial y}\right)\Delta t + \frac{1}{2}\frac{\partial}{\partial y}\left(BB\frac{\partial U}{\partial y}\right)\Delta t^2 + O(\Delta t^3) \tag{32}$$

$$L_z; U^{n+1} = U^n - C\left(\frac{\partial U}{\partial z}\right)\Delta t + \frac{1}{2}\frac{\partial}{\partial z}\left(CC\frac{\partial U}{\partial z}\right)\Delta t^2 + O(\Delta t^3). \tag{33}$$

Equation (24) is identical to the fractional step formulation applied to the electric and magnetic field intensities U,

$$U^{n+2} = L_x L_y L_z L_z L_y L_x U^n. \tag{34}$$

It is more advantageous to demonstrate the numerical accuracy of the present method using Eq. (34). This basic formulation eliminates tedious algebraic manipulations of the characteristics between coordinates.

The gist of the fractional-step or the time splitting scheme can be viewed as a temporal integration procedure, in that the time advancement of a solution is an accumulative process by adding the contributions from the split terms consecutively. The individual fractional steps only provide a partial approximation to the equation. Only after a complete symmetric and cyclic sequence, the approximation will yield a second-order method in time. The specifics follow:

$L_x(U)$;

$$U^{n+1/3} = U^n - A\left(\frac{\partial U}{\partial x}\right)\Delta t + \frac{1}{2}\frac{\partial}{\partial x}\left(AA\frac{\partial U}{\partial x}\right)\Delta t^2 + O(\Delta t^3) \tag{35}$$

$L_y L_x(U)$;

$$U^{n+2/3} = U^n - \left(A\frac{\partial U}{\partial x} + B\frac{\partial U}{\partial y}\right)\Delta t + \frac{1}{2}\left[\frac{\partial}{\partial x}\left(AA\frac{\partial U}{\partial x}\right) + \frac{\partial}{\partial y}\left(BB\frac{\partial U}{\partial y}\right) + 2\frac{\partial}{\partial y}\left(BA\frac{\partial U}{\partial x}\right)\right]\Delta t^2 + O(\Delta t^3) \tag{36}$$

$L_zL_yL_x(U)$;

$$U^{n+1} = U^n - \left(A\frac{\partial U}{\partial x} + B\frac{\partial U}{\partial y} + C\frac{\partial U}{\partial z}\right)\Delta t + \frac{1}{2}\left[\frac{\partial}{\partial x}\left(AA\frac{\partial U}{\partial x}\right) + \frac{\partial}{\partial y}\left(BB\frac{\partial U}{\partial y}\right) + \frac{\partial}{\partial z}\left(CC\frac{\partial U}{\partial z}\right) + 2\frac{\partial}{\partial y}\left(BA\frac{\partial U}{\partial x}\right) + 2\frac{\partial}{\partial z}\left(CA\frac{\partial U}{\partial x}\right) + \frac{\partial}{\partial z}\left(CB\frac{\partial U}{\partial y}\right)\right]\Delta t^2 + O(\Delta t^3) \quad (37)$$

$L_zL_zL_yL_x(U)$;

$$U^{n+4/3} = U^n - \left(A\frac{\partial U}{\partial x} + B\frac{\partial U}{\partial y} + 2C\frac{\partial U}{\partial z}\right)\Delta t + \frac{1}{2}\left[\frac{\partial}{\partial x}\left(AA\frac{\partial U}{\partial x}\right) + \frac{\partial}{\partial y}\left(BB\frac{\partial U}{\partial y}\right) + 4\frac{\partial}{\partial z}\left(CC\frac{\partial U}{\partial z}\right) + 2\frac{\partial}{\partial y}\left(BA\frac{\partial U}{\partial x}\right) + 4\frac{\partial}{\partial z}\left(CA\frac{\partial U}{\partial x}\right) + \frac{\partial}{\partial z}\left(CB\frac{\partial U}{\partial y}\right)\right]\Delta t^2 + O(\Delta t^3) \quad (38)$$

$L_yL_zL_zL_yL_x(U)$;

$$U^{n+5/3} = U^n - \left(A\frac{\partial u}{\partial x} + 2B\frac{\partial U}{\partial y} + 2C\frac{\partial U}{\partial z}\right)\Delta t + \frac{1}{2}\left[\frac{\partial}{\partial x}\left(AA\frac{\partial U}{\partial x}\right) + 4\frac{\partial}{\partial y}\left(BB\frac{\partial U}{\partial y}\right) + 4\frac{\partial}{\partial z}\left(CC\frac{\partial U}{\partial z}\right) + 4\frac{\partial}{\partial y}\left(BA\frac{\partial U}{\partial x}\right) + 4\frac{\partial}{\partial y}\left(BC\frac{\partial U}{\partial z}\right) + 4\frac{\partial}{\partial z}\left(CA\frac{\partial U}{\partial x}\right) + 4\frac{\partial}{\partial z}\left(CB\frac{\partial U}{\partial y}\right)\right]\Delta t^2 + O(\Delta t^3) \quad (39)$$

and, finally,

$L_xL_yL_zL_zL_yL_x(U)$;

$$U^{n+2} = U^n - \left(A\frac{\partial U}{\partial x} + B\frac{\partial U}{\partial y} + C\frac{\partial U}{\partial z}\right)(2\Delta t) + \frac{1}{2}\left[\frac{\partial}{\partial x}\left(AA\frac{\partial u}{\partial x}\right) + \frac{\partial}{\partial y}\left(BB\frac{\partial U}{\partial y}\right) + \frac{\partial}{\partial z}\left(CC\frac{\partial U}{\partial z}\right) + \frac{\partial}{\partial x}\left(AB\frac{\partial U}{\partial y}\right) + \frac{\partial}{\partial x}\left(AC\frac{\partial U}{\partial z}\right) + \frac{\partial}{\partial y}\left(BA\frac{\partial U}{\partial x}\right) + \frac{\partial}{\partial y}\left(BC\frac{\partial U}{\partial z}\right) + \frac{\partial}{\partial z}\left(CA\frac{\partial U}{\partial x}\right) + \frac{\partial}{\partial z}\left(CB\frac{\partial U}{\partial y}\right)\right](2\Delta t)^2 + O(\Delta t^3). \quad (40)$$

The above numerical approximation to Eq. (3) and the equivalence to Eq. (24) yields the identical expression to that of a straightforward Taylor series expansion up to the order of Δt^3. The second-order spatial approximation was adopted for the present purpose, as shown by Eqs. (22) and (23). Therefore, the present method for solving the Maxwell equations will produce the second-order accurate approximation in time and space after the symmetric and cyclic operator sequence.

Since one-dimensional characteristics of the Maxwell equations are completely uncoupled from each other and appear in scalar form, the one-dimensional Riemann formulation is exact (Eqs. (19), (20), and (21)). However, the most important feature of the present numerical procedure is that the costly matrix inversion for implicit formulation becomes unnecessary. Using windward discretization, the difference in computational effort between implicit and explicit procedures diminishes. Both use the forward or backward substitution to advance the solution to the next time level. Three numerical procedures have been developed. Two codes are based on the implicit and explicit fractional-step scheme. The third procedure is the unsplit explicit version which closely resembles conventional applications [2].

The fractional-step algorithm is best described in terms of a succession of approximate solutions in each spatial dimension. Under quite general circumstances, the numerical procedure is unconditionally stable if all one-dimensional differencing operators possess this feature [16, 17]. Since the property of upwind model wave equations are well established by Warming and Beam [11, 15], the details will not be reported here. Like all approximate factored methods for solving multidimensional problems, there is ambiguity in describing intermediate temporal data in the cyclic solving sequence [11, 14–17]. The issues of well-posedness [21, 22] and physically meaningful temporal data [3, 4] at the intermediate time steps will be further studied.

II.3. *The Imposed Conditions at Truncated Boundaries*

In the present analysis, the finite differencing is implemented to honor the physical orientation of wave motion. In general, information is propagated from the interior/exterior of the computational domain to the boundary along the characteristics. The characteristic equations are really the compatibility relationships and are equally applicable on the boundaries of the computational domain [3, 4, 6, 22]. Therefore, in order to eliminate the interior wave reflection from the truncated computational domain, only the null value of incoming characteristic variables from far field need to be specified on the numerical boundaries:

$$W_{x,n} = 0, \quad x < 0 \text{ and } x > 1 \quad (41)$$

$$W_{y,n} = 0, \quad y < 0 \text{ and } y > 1 \quad (42)$$

$$W_{z,n} = 0, \quad z < 0 \text{ and } z > 1. \quad (43)$$

This boundary condition is well-posed and exact when the characteristic variable is aligned with the wave motion. For

electromagnetic wave propagation, the direction is always known to be perpendicular to both the electric and magnetic fields. However, in the present investigation, the coordinate transformation has not been implemented. Therefore, the exact no-reflection boundary condition will be degenerated to an approximation when the wave motion is not aligned with the Cartesian frame.

III. NUMERICAL PROCEDURE

Numerical simulations of the present investigation are performed in a truncated computational domain defined by a cube. All spatial variables X, Y, and Z have the same range of zero to unity. The temporal variation is therefore scaled by the wave speed and spatial dimension through the CFL number, $\lambda \Delta t / \Delta x$. For the temporally and spatially second-order accurate scheme, the formal truncation error will have an order of magnitude of 1×10^{-4} for a mesh spacing around $\frac{1}{50}$.

As a validation of numerical procedure, the electromagnetic wave propagation within a three-dimensional rectangular wave guide and a radiating field of an oscillating electric dipole were simulated. All numerical results were generated on an IRIS 4D/440VGS workstation. On mesh systems of $45 \times 45 \times 45$ or $46 \times 46 \times 46$, the implicit and the explicit fractional-step, as well as the unsplit explicit procedure, yielded a consistent data processing rate of 2.71×10^{-4} s, 2.93×10^{-4} s, and 3.35×10^{-4} s, respectively. Using a standard compiler option, the two fractional-step methods attained a parallel efficiency about 0.75, operating on four nodes. Timing information of the unsplit explicit method in parallel computing was not collected.

The implicit fractional-step method has an unlimited theoretical stability limit. However, at a CFL value greater than five, the dispersive numerical error became pronounced over a wide range of wave numbers for all problems investigated. On the other hand, the upper stability bound of the explicit fractional-step method was sustained at a CFL number of two. At CFL numbers of unity and two, the perfect shift condition of numerical solution by the explicit method is achieved at certain conditions. Under this circumstance, the upwind procedure is at least fourth-order accurate in space when supported by a uniform mesh system. The unsplit explicit method has the most restricted stability constraint; the CFL number used during the present analysis was consistently less than the maximal value of $2/\sqrt{3}$.

Since all wave motions were studied under periodic conditions, the property of temporal accuracy can be verified easily by examining the periodicity of wave propagation. A characteristic time scale is defined by the time elapse for an electromagnetic pulse to travel through the computational domain. All numerical results are capable of duplicating the periodic identity within the truncation error $O(10^{-4})$. This accuracy was retained for the oscillating electric dipole even after 690 time steps. The time interval corresponds to the physical situation that 30 waves had been generated and passed through the computational domain. Based on this fact, all numerical results to be presented in the following discussions are randomly selected instantaneous values of a dynamic event.

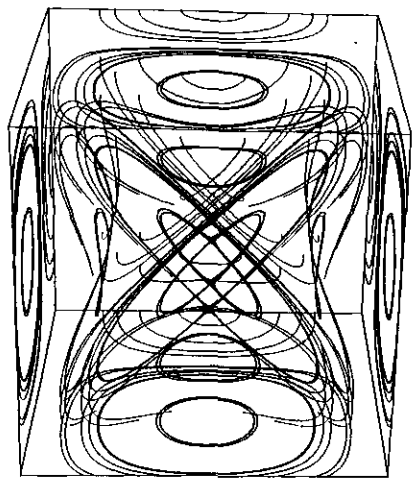

FIG. 1. Magnetic field of a 3D wave guide: CFL = 1.0; Tch = 1.0; A = B = π; $\omega = 2\pi$.

IV. DISCUSSION OF NUMERICAL RESULTS

IV.1. *Electromagnetic Wave within a Three-Dimensional Wave Guide*

The wave motion confined within a three-dimensional rectangular wave guide was first simulated. For this phenomenon, the closed form solution of time-dependent Maxwell equations is known [20, 23]. The 3D electromagnetic wave is specified to propagate along the Z coordinate, thus all the components of electric and magnetic intensities contain a common sinusoidal function of time and Z. In a degenerated two-dimensional setting, this problem is commonly designated as the $TE_{1,1}$ transverse electric wave [20, 23]. The initial and boundary conditions were prescribed as follows: The incoming incident wave was completely specified at computational boundary for each time step. The exact characteristic-based no-reflection condition was imposed at the exit plane $Z = 1$, Eq. (24). In order to focus attention on the validation of numerical methods and the characteristic-based no-reflection condition, all boundary values on the cross section planes were over-specified from the analytic solution.

In Figs. 1 and 2, the perspective views of the entire magnetic and electric field are presented, respectively. The magnetic field exhibits a complex three-dimensional structure. The magnetic lines on the wave guide surfaces coincide with the exact solution of $TE_{1,1}$ wave. The electric field appears as a collection of identical planar formations, as a transverse electric wave in a rectangular guide should [20, 23]. From these two figures, the overall electromagnetic field structure of the numerical simulations was confirmed by the classic result.

In Fig. 3, the theoretical and computed electromagnetic fields

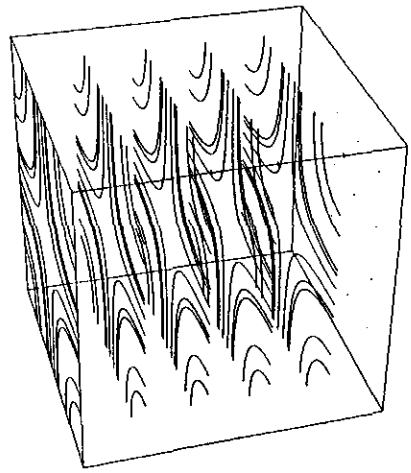

FIG. 2. Electric field of a 3D wave guide: CFL = 1.0; Tch = 1.0; A = B = π; $\omega = 2\pi$.

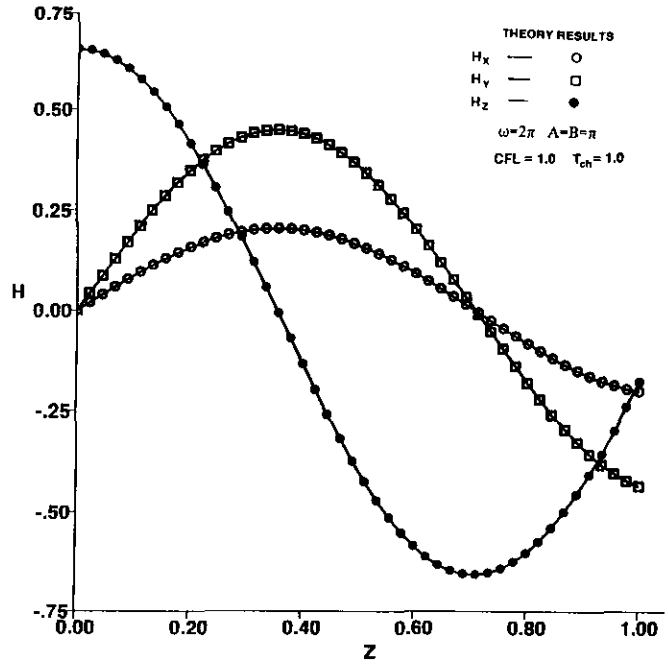

FIG. 4. Solutions of magnetic field component in a 3D wave guide.

are projected on a $Z = 0.5$ (X–Y cross section) plane to facilitate a direct comparison. The electric field is traced by solid lines, and the magnetic field is depicted by dots. First, the analytic and numerical results are identical within plotting error. This affinity is preserved for each and every cross-sectional plane within the computational domain. There is also no detectable discrepancy between the two solutions of implicit and explicit fractional-step methods. This observation substantiates the fact that the present procedures are capable of generating an accurate numerical simulation with well-posed boundary conditions. As additional evidence, the orthogonal condition is maintained between the electric and magnetic fields over the entire cross-sectional plane.

The instantaneous values of three components of magnetic field intensity are given in Fig. 4. The magnetic field distribution is selected from a set of X and Y coordinates over the entire range of Z. Since the numerical results from both implicit and explicit fractional-step methods are identical to within the same order of magnitude of truncation error, only a set of numerical results are included for the purpose of comparison. It is obvious that the numerical results agree completely with the analytic expression. Particularly, the wave passes through the computational boundary without any indication of the induced reflection from the artificial boundary.

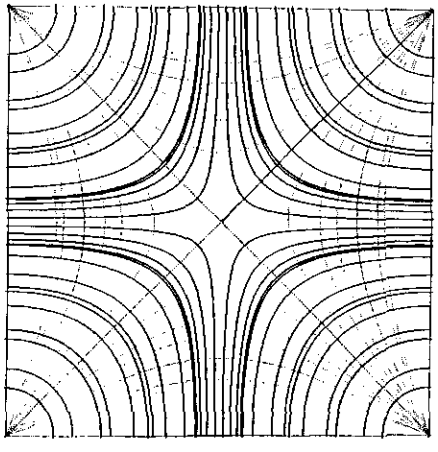

FIG. 3. Electromagnetic field projection of a 3D wave guide: CFL = 1.0; Tch = 1.0; A = B = π; $\omega = 2\pi$.

The corresponding electric field is presented in Fig. 5. For the transverse electric wave, the Z component of electric intensity vanishes identically for both analytic and numerical results. Again the agreement between analytic and numerical solutions is excellent. Most importantly, the characteristic-based no-reflection boundary condition has been demonstrated to be accurate. In fact, this boundary condition on the truncated computational domain is exact for the investigated phenomenon and is the best achievable by numerical means.

IV.2. *The Oscillating Electric Dipole*

The solution of an electromagnetic wave induced by an oscillating electric dipole was attempted next. The closed form solution to the time-dependent, three-dimensional Maxwell equation is also known [20, 23]. However, it is a solution obtained by a limiting process which contains a singular behavior at the dipole. The leading term singularity of field variables appears as the inverse cubic power of radial distance from the dipole.

The numerical simulation of the oscillating electric dipole was generated by an alternating current vector, $J_z = \sin(2\pi * t)$

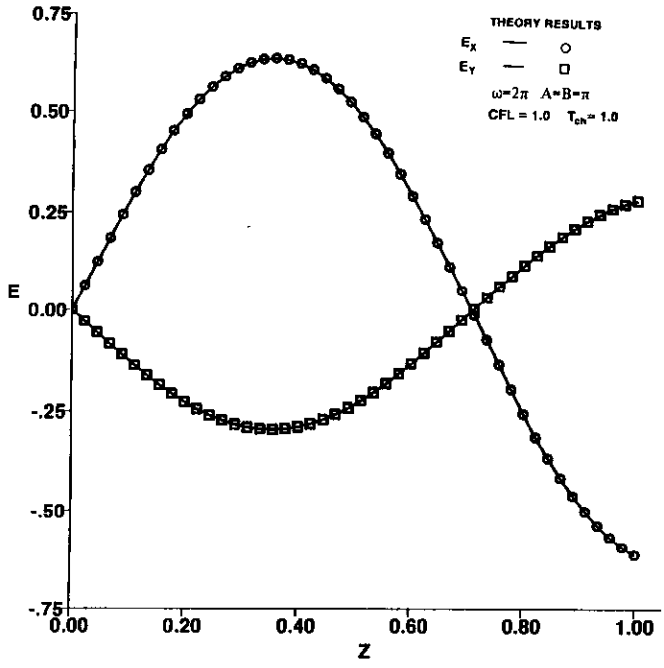

FIG. 5. Solutions of electric field component in a 3D wave guide.

located at the center of a $45 \times 45 \times 45$ uniform mesh computational domain. The calculations were obtained without the advantage of a coordinate transformation to map the computational space into a spherical field. The principal axis of the radiating wave was not aligned with any coordinates of the Cartesian frame. Therefore, the present characteristic-based no-reflection condition at best is only an approximation at the outer edges of the computational domain.

In Fig. 6, the computed Z components of the oscillating electric field by the explicit and implicit schemes are given. These isoelectrics were sampled when the first wave front was exiting the computational domain. The selected 2D projection contained the dipole in a bisecting plane of the entire space. It is apparent that the numerical solution of the explicit fractional-step method has incurred the grid decoupling phenomenon discovered recently by Ray [24]. However, the solution of the implicit fractional-step method, generated under identical conditions as that of the explicit scheme, yielded a physically meaningful solution. In addition, the distortion of reflecting waves from artificial boundaries by the characteristic-based formulation is significantly restrained.

The computed circumferential component of the electric intensity by the implicit fractional-step method and the accompanying analytic results are depicted in Fig. 7. The three-point upwind differencing formulation demonstrated a robust stability property even for a phenomenon that contains singular behavior. Except in the immediately adjacent regions of the dipole, the agreement between analytic and numerical results is reasonable. Similar comparisons of the radial component of electric and the azmuthal component of magnetic intensities with theoretical expressions were also obtained. The specific and overall behavior of the total field is nearly identical and is not included here. The scaling law of the singular dipole behavior is known to be the inverse cubic power of the distance from the dipole; a linear mesh spacing refinement may not be effective to improve the numerical resolution. Therefore, no additional enriched grid computation was performed.

The peculiar grid decoupling numerical behavior of the explicit scheme was a recent finding by Ray [24] and was substantiated by the present explicit solution. In the context of the present study, this numerical oddity is understandable on the framework of characteristic formulation. From eigenvalue analysis, all pertaining data are transmitted by a preferred direction. The single point pulse generated by the dipole lacks a directional bias that is required by the explicit method in solving the initial value problem. The directional numerical sweep by the explicit method creates at least two partial null data strings separated by the single dipole, Eqs. (19) and (20). The implicit algorithm, on the other hand, has to share information from boundary to boundary at an advanced time level. The grid decoupling phenomenon is completely avoided. Therefore, it is surmised that the grid decoupling may be induced by the deficient initial condition for the explicit scheme. As a direct support to the fact that the numerical anomaly is not associated uniquely with the explicit fractional-step method, calculations by the unsplit explicit method also exhibit a similar but different grid decoupling pattern. The final substantiation to the present conjuncture is derived from the following numerical experiments.

The oscillating electric dipoles were again simulated by the implicit and explicit fractional-step methods, as well as an unsplit explicit scheme on a $46 \times 46 \times 46$ mesh system. The periodic electric dipole was then imposed from the analytic result on two contiguous points in the middle of the computational domain, instead of a single point current source. The rest of the simulation conditions remained unaltered. All the numerical results, either by the implicit or two explicit methods, are nearly identical and do not contain any numerical patterns of grid decoupling. The new evidence is sufficient for the present purpose; however, this unique behavior may warrant additional in-depth investigations.

The comparison of computed and analytic azimuthal components of magnetic intensity is displayed in Fig. 8. The agreement of three numerical results and the theory is reasonable. The lack of numerical resolution is clearly demonstrated in the transitional region of near and far field, where the gradient of variable, and, thus, the truncation error reaches its maximum magnitude. The instantaneous values of magnetic intensity were selected along a radial ray that aligned with the X coordinate. There were small deviations in far field solutions along the radial rays with different azimuthal and meridian angles. However, these discrepancies were less than the differences between solutions of the three methods.

In Fig. 9, the comparison of calculated radial components

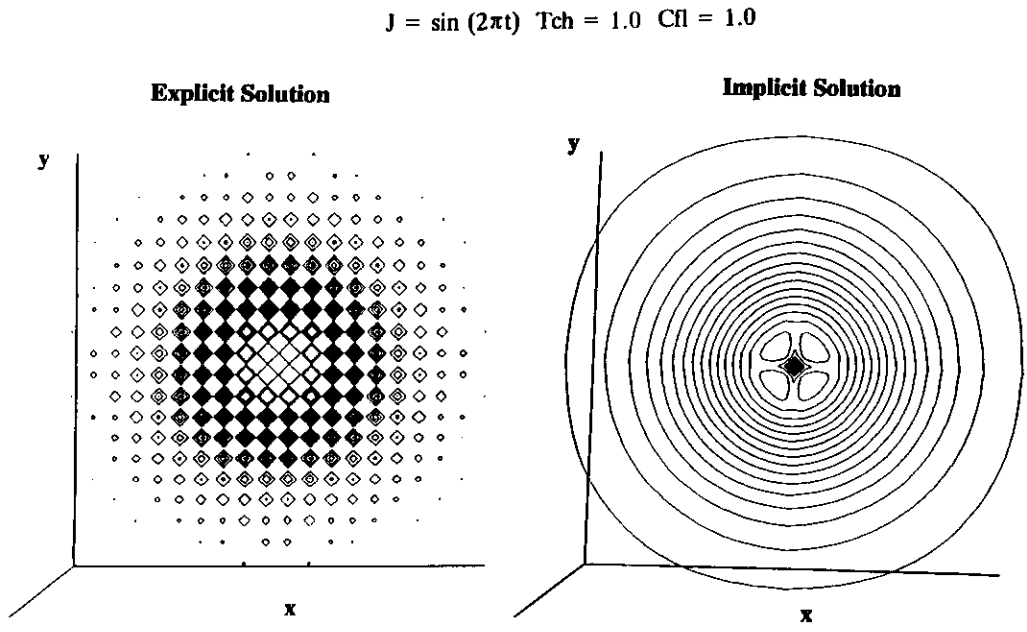

FIG. 6. E_z contours of a dipole in $Z = 0.5$ plane: $J = \sin(2\pi t)$; Tch = 1.0; CFL = 1.0.

of electric field intensity with analytic results is presented. Again, the only significant difference from theory was observed in the near to far field transition region. The difference between solutions of the three numerical procedures was only a fraction of 1%.

The comparison of the circumferential component of electric intensity and theory is depicted in Fig. 10. From the theory, this field component has the widest variation among all existing electromagnetic waves. The unsplit explicit method yielded the least discrepancies from the theoretical results over the entire range of r, as a consequence of containing no splitting error. However, all numerical solutions were generated at a CFL

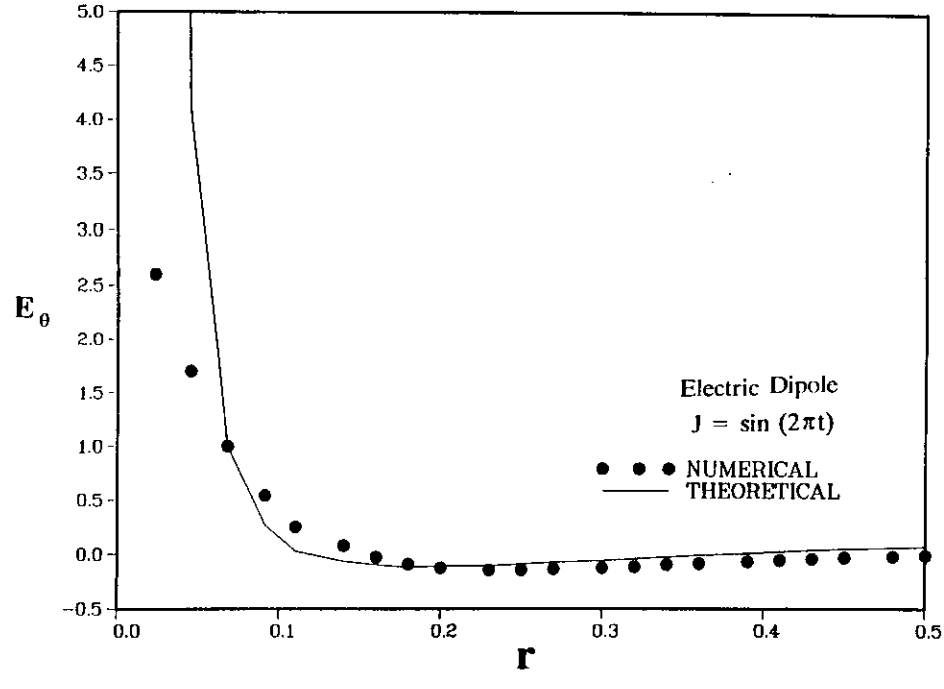

FIG. 7. Computed electric circumferential component of a dipole.

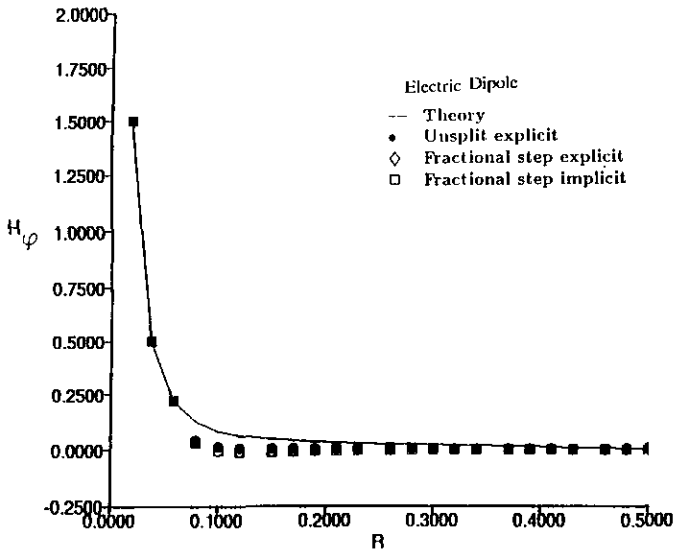

FIG. 8. Comparison of magnetic azimuthal components of a dipole.

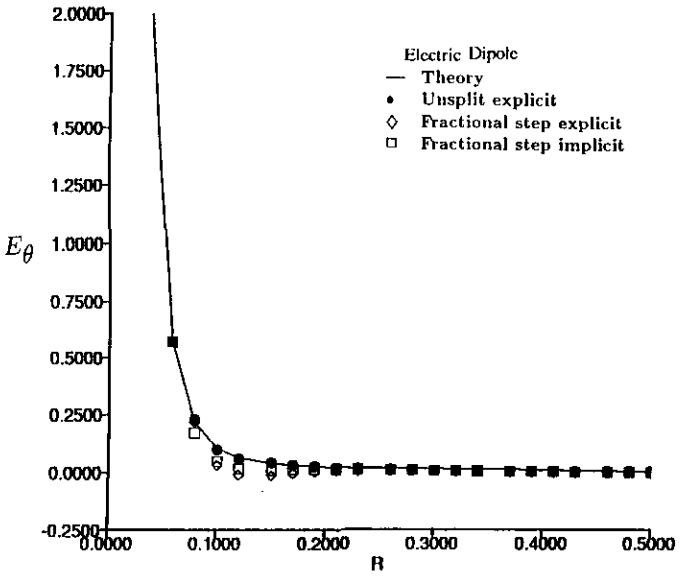

FIG. 10. Comparison of electric circumferential components of a dipole.

value of 0.5 to sustain the stable calculations for the unsplit scheme. At this CFL value, both fractional-step methods were not operated at the optimal condition for the minimum dissipative and dispersive errors.

The entire magnetic field results computed by the implicit fractional-step and the theoretical result are compared side-by-side in Fig. 11. The instantaneous time exposure was taken when the second pulse was exiting the computational space. The traces of magnetic field intensity were constrained to a series of planar concentric circles perpendicular to the direction of the alternating current point source. Significant departure from a two-dimensional structure appeared only in the location adjacent to the singular dipole. This behavior was verified by the specific and detailed comparison given in Fig. 8. In all, the numerical simulation has demonstrated a creditable degree of fidelity to physics.

In Fig. 12, a perspective view of complete electric fields of the dipole from the computed and the analytic result are presented. The orderly loops originating from the dipole and streaks around them indicate a composite field of two predominant radial and circumferential components. The topology between the theoretical and numerical results is similar, except in the corner regions of the computational cube. In these regions, the one-dimensional characteristic-based no-reflection boundary condition becomes increasingly inaccurate. The intricate electric field structures in the corner regions are not captured

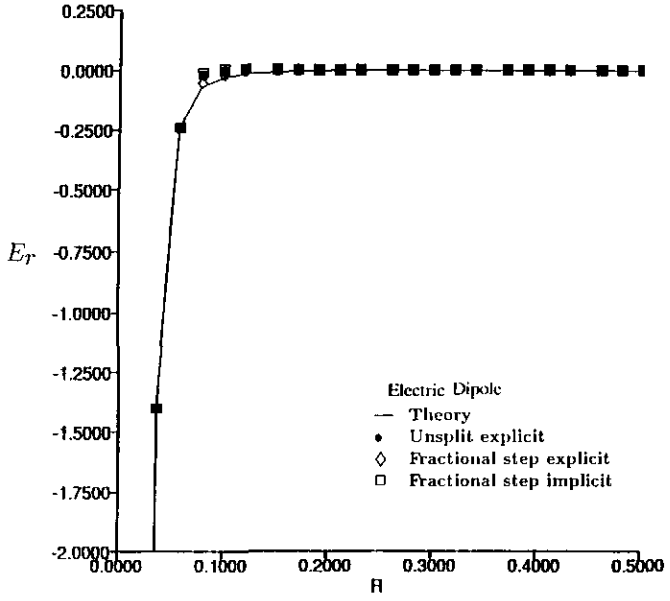

FIG. 9. Comparison of electrical radial components of a dipole.

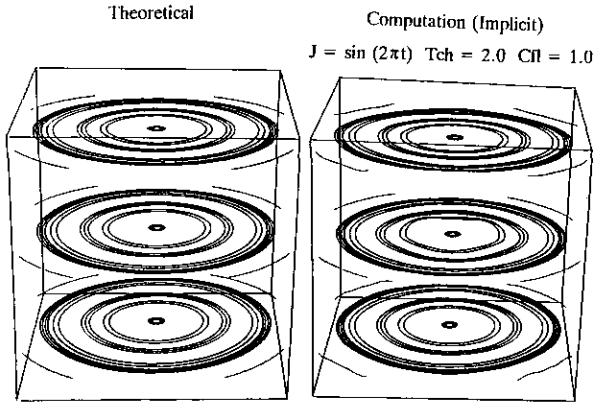

FIG. 11. Comparison of magnetic fields of a dipole.

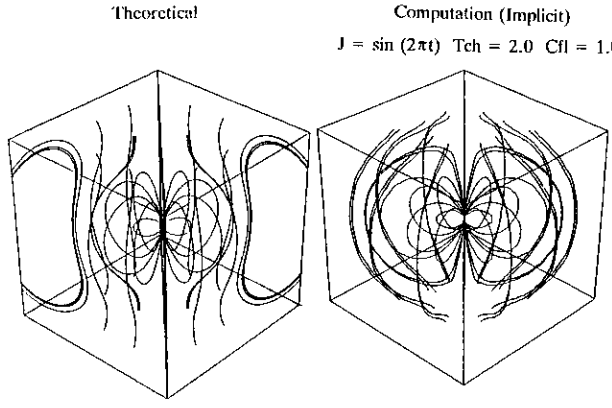

FIG. 12. Comparison of electric fields of a dipole.

by the numerical simulation. This observation is true for all three numerical results using different techniques. From the detailed comparisons of the electric field, Figs. 9 and 10, the deviation between numerical and theoretical results is less than a fraction of 1%. Therefore, the field feature at the corner is believed to be a secondary structure induced by the numerical error at the boundary.

Improvement of the numerical accuracy can be achieved through a coordinate transformation to a general curvilinear system. In the transformed coordinates, the characteristic data can always be effectively utilized to construct the exact no-reflection condition. Near the outer edge of the computational domain, the coordinates can be mapped to align with the axis of wave motion [20, 23]. In addition, the grid spacing also can be controlled to meet any particular scaling law for accurate numerical results.

V. CONCLUDING REMARKS

Two characteristic-based, fractional-step, implicit, and explicit methods have been successfully developed for solving three-dimensional, time-dependent Maxwell equations. Under controlled conditions, these numerical procedures generated excellent solutions for a three-dimensional wave guide, in comparison with the theoretical result. Reasonable simulations of an oscillating electric dipole were also obtained. The characteristic-based no-reflection condition, imposed at the control surfaces of computational domain, has exhibited a degree of effectiveness beyond its range of validity. For the present investigation, the grid decoupling numerical anomaly of the explicit schemes has been illustrated as a consequence of ill-posed initial conditions.

Additional efforts have been planned to develop the formulation on general curvilinear coordinates and to map onto massively parallel computers.

ACKNOWLEDGMENTS

Stimulating discussions and assistance from Drs. D. Gaitonde and K. Hill are gratefully acknowledged.

REFERENCES

1. A. Taflove, AIAA Preprint 92-0333, January 1992 (unpublished).
2. V. Shankar, AIAA Preprint 91-0002, January 1991 (unpublished).
3. J. S. Shang, AIAA Preprint 92-0452, January 1992 (unpublished).
4. J. S. Shang, AIAA Preprint 91-0606, January 1991 (unpublished).
5. D. A. Anderson, AFATL-TR-88-1987, AF Armament Laboratory, Eglin Air Force Base, June 1989 (unpublished).
6. A. Sommerfeld, *Partial Differential Equations in Physics* (Academic Press, New York, 1949).
7. B. Enquist and A. Majda, *Math Comput.* **31,** 629 (1977).
8. G. Muir, *IEEE Trans. Electromag. Comput.* **EMC-23**(4), 377 (1981).
9. J. L. Steger and R. F. Warming, *J. Comput. Phys.* **40**(2), 263 (1981).
10. P. L. Roe, *Annu. Rev. Fluid Mech.* **18,** 337 (1986).
11. D. A. Anderson, J. C. Tannehill, and R. H. Pletcher, *Computational Fluid Dynamics and Heat Transfer* (Hemisphere, Washington, DC/New York/ McGraw–Hill, New York, 1984).
12. J. Douglas and J. Gunn, *Numer. Math.* **6,** 428 (1965).
13. R. F. Warming and R. M. Beam, *SIAM-AMS Proc.* **11,** 85 (1978).
14. R. D. Richtmyer and K. W. Morton, *Difference Methods for Initial-Value Problems,* 2nd ed. (Interscience, New York, 1967).
15. R. F. Warming and R. M. Beam, "Upwind Second-Order Difference Schemes and Applications in Unsteady Aerodynamic Flows," in *Proceedings AIAA 2nd Comput. Fluid Dynamics Conf., Hartford, CN, 1975,* p. 17 (unpublished).
16. K. A. Bagrinovskii and S. K. Godunov, *Dokl. Akad. Nauk USSR* **115,** 431 (1957).
17. N. N. Yanenko, *Sibirsk. Math. Zh.* **5,** 1430 (1964).
18. S. S. Abarbanel, D. L. Dwoyer, and D. Gotlieb, ICASE No. 82-39, 1982 (unpublished).
19. S. X. Ying, Ph.D. dissertation, Stanford University, June 1986 (unpublished).
20. R. R. Harrington, *Time-Harmonic Electromagnetic Fields* (McGraw–Hill, New York, 1961).
21. H. O. Kreiss, *Commun. Pure Appl. Math.* **22,** 277 (1970).
22. R. Courant and D. Hilbert, *Methods of Mathematical Physics.* Vol. II. *Partial Differential Equations* (Interscience, New York, 1965).
23. E. C. Jordan, *Electromagnetic Waves and Radiating System* (Prentice-Hall, Englewood Cliffs, NJ, 1960).
24. S. L. Ray, *IEEE Trans. Antennas Propag.* **40**(4), 443 (1992).